

Responses to the comments from Anonymous Referee #2

We are very grateful to the reviewer for the positive and careful review. The thoughtful comments have helped improve the manuscript. The reviewer's comments are italicized and marked in blue, and our responses immediately follow.

In this revised manuscript, the authors have successfully addressed my major concerns in my previous review. Most importantly, they are using global temperature changes instead of local ones. They also included a 3 degree limit additionally to 1.5 and 2. Both of these improvements significantly increase the appeal of the manuscript to a wider readership. The manuscript is overall well written. I still find that the methods, in detail the processing of the input data, is not described enough (see major comments below). As a result, I still recommend major revisions. However, I believe that the authors should face no difficulties providing this additional information and the manuscript can be published subsequently.

Response: Thanks for your careful review and positive comments, and we are glad to see the revised manuscript has met your major comments and suggestions. We have now added an appendix to clarify data processing methods. Please see our responses below for details.

Major comment:

1. 117ff: This paragraph describes the processing of the data set. Important details are not mentioned. Questions that need to be answered are:

- 1.) How are CMIP5 data and observations interpolated?*
- 2.) How was the correction method by Li et al. modified?*
- 3.) How was daily precipitation and temperature disaggregated to 6-hourly resolution using CRUNCEP data?*
- 4.) It should be mentioned clearly that only precipitation and temperature have been used from the CMIP5 models.*
- 5.) What does it mean that other variables have been taken from CRUNCEP? Have these been resampled somehow? Have climatological values been used?*

The last question regarding direct use of CRUNCEP data is critical because it is not clear whether physical consistency among forcing variables is maintained. For example, is shortwave radiation influenced by precipitation? Please comment. Please also mention this as a limitation of the study that it is unclear how the climate change signal by GCMs might be affected by using CRUNCEP data for a majority of forcing variables.

These details can be provided in an appendix.

Response: Thanks for the comments and suggestions. We have now added an Appendix Section for these details as follows:

“Appendix: Details of Processing Climate Forcings

The land surface hydrological model CLM-GBHM requires a list of input climate forcings, i.e. precipitation, near surface air temperature, incident solar radiation, air pressure, specific humidity and wind speed. These variables were generated from three datasets in this study: CMIP5 daily simulations during both historical (1961-2005) and future (2006-2099) periods, CRUNCEP 6-hourly dataset during 1959-2005, and China Meteorological Administration (CMA) daily station observations during 1961-2005. All datasets were firstly regridded to the same resolution (0.01 degree) by using bilinear interpolation method for further processing.

After spatial interpolation, daily precipitation and temperature from CMIP5 simulations were adjusted to remove their monthly biases compared to CMA observations, by applying a correction method to each model at each grid cell separately. This method modified the widely used quantile-mapping method (CDFm) and processed historical and future timeseries in different ways. For historical period, bias-corrected monthly variable x (i.e., precipitation or temperature) was calculated based on CDFm:

$$x_{sim, his, corrected} = F_{obs, his}^{-1} (F_{sim, his} (x_{sim, his, biased})), \quad (A1)$$

where F is cumulative distribution function of variable x , subscripts sim , obs , his , $biased$, $corrected$ represent simulated value, observed value, historical period, value with bias and value after bias correction at monthly scale, respectively. The basic assumption of CDFm is that the climate distribution does not change much over time, however, this is invalid considering intense global warming in the future. Therefore, an equidistant CDF matching method (EDCDFm; Li et al., 2010) was applied for future projections, which assumes that the difference between simulated and observed values remains the same over time:

$$x_{sim, fut, corrected} = x_{sim, fut, biased} + F_{obs, his}^{-1} (F_{sim, fut} (x_{sim, fut, biased})) - F_{sim, his}^{-1} (F_{sim, fut} (x_{sim, fut, biased})), \quad (A2)$$

where subscript fut represents future period. After bias correction at monthly scale, new daily precipitation (temperature) series were generated based on the ratio (difference) between the new and old CMIP5 simulated monthly means:

$$P_{d, corrected} = (P_{m, corrected} / P_{m, biased}) \cdot P_{d, biased}, \quad (A3)$$

$$T_{d, corrected} = (T_{m, corrected} - T_{m, biased}) + T_{d, biased}, \quad (A4)$$

where P and T represent precipitation and temperature, subscripts d and m represent daily value and corresponding monthly mean, respectively.

In order to temporally disaggregate daily temperature and precipitation to a 6-hours interval during both historical and future periods, the diurnal cycle information from CRUNCEP dataset was introduced. By looping the CRUNCEP data during 1959-2005 (47 years) twice, we could also generate “future data” (2006-2099, 94 years). By

using the same disaggregation method that downscales variables from monthly to daily, temporal downscaling from daily to 6-hourly scales was achieved:

$$P_{6h,corrected} = (P_{d,corrected} / P_{d,CRUNCEP}) \cdot P_{6h,CRUNCEP}, \quad (A5)$$

$$T_{6h,corrected} = (T_{d,corrected} - T_{d,CRUNCEP}) + T_{6h,CRUNCEP}, \quad (A6)$$

where subscript *6h* represents 6-hourly values. It should be mentioned that only precipitation and temperature have been used from CMIP5 models, with other climate forcing variables (i.e., incident solar radiation, air pressure, specific humidity and wind speed series) directly taken from CRUNCEP dataset. Whether physical consistency among all climate forcing variables was maintained or not by simply introducing CRUNCEP dataset was not considered in this study, and it is unclear how the climate change signals by GCMs might be affected by using CRUNCEP data for a majority of forcing variables. Although resampling methods (e.g., Schaake Shuffle) that are widely used in temporal downscaling for seasonal forecasting might result in more consistent forcing variables, whether such consistency (e.g., temperature-humidity relationship) holds for future projection given the changing climate is unknown. More sophisticated downscaling techniques (either statistical or dynamical) are needed for further studies.” (L417-464)

l. 342ff: In this paragraph, please do not refer to warming levels because those conflict with the RCP scenarios. For example, warming levels are reached at different RCP scenarios at different points in time. A statement such as that (l. 344ff: "RCPs scenario uncertainty accounts for 14.3% of temperature uncertainty at 1.5 °C warming level with this proportion increasing to 33% (63.7%) at 2 °C (3 °C) warming level, while its contribution to precipitation uncertainty remains less than 10%.") makes no sense because some RCP scenarios will not reach 3 degrees. Please also remove the dashed lines indicating when the ensemble reaches a warming level from Fig. 8.

Response to R2C2: Thanks for your advice. We have removed the words referring to warming levels in this paragraph, the dashed lines in Figure 8, as well as Table 4.

Minor comments:

l. 342: "Model accounts..." . Please be more specific here and write "GCM and land surface hydrological model ..."

Response to R2C3: Thanks for the comment and we have revised it as suggested.

1 **More Severe Hydrological Drought Events Emerge at Different Warming Levels**
2 **over the Wudinghe Watershed in northern China**

3 Yang Jiao^{1,2}, Xing Yuan^{1,2*}

4 ¹School of Hydrology and Water Resources, Nanjing University of Information

5 Science and Technology, Nanjing, 210044, Jiangsu, China

6 ²Key Laboratory of Regional Climate-Environment for Temperate East Asia

7 (RCE-TEA), Institute of Atmospheric Physics, Chinese Academy of Sciences, Beijing,

8 100029, China

9
10 *Hydrology and Earth System Sciences*

11 Submitted May 8, 2018

12 Revised ~~December 24~~[September 29](#), 2018

13

*Corresponding author address: Xing Yuan, School of Hydrology and Water Resources, Nanjing University of Information Science and Technology, Nanjing, 210044, Jiangsu, China. E-mail: xyuan@nuist.edu.cn

14 **Abstract**

15 Assessment of changes in hydrological droughts at specific warming levels is
16 important for an adaptive water resources management with consideration of the 2015
17 Paris Agreement. However, most studies focused on the response of drought
18 frequency to the warming and neglected other drought characteristics including
19 severity. By using a semiarid watershed in northern China (i.e., Wudinghe) as an
20 example, here we show less frequent but more severe hydrological drought events
21 emerge at 1.5, 2 and 3 °C warming levels. We used meteorological forcings from eight
22 Coupled Model Intercomparison Project Phase 5 climate models under four
23 representative concentration pathways, to drive a newly developed land surface
24 hydrological model to simulate streamflow, and analyzed historical and future
25 hydrological drought characteristics based on the Standardized Streamflow Index. The
26 Wudinghe watershed will reach the 1.5/2/3 °C warming level around
27 2015-2034/2032-2051/2060-2079, with an increase of precipitation by 8%/9%/18%
28 and runoff by 27%/19%/44%, and a drop of hydrological drought frequency by
29 11%/26%/23% as compared to the baseline period (1986-2005). However, the drought
30 severity will rise dramatically by 184%/116%/184%, which is mainly caused by the
31 increased variability of precipitation and evapotranspiration. The climate models and
32 the land surface hydrological model contribute to more than 80% of total uncertainties
33 in the future projection of precipitation and hydrological droughts. This study
34 suggests that different aspects of hydrological droughts should be carefully
35 investigated when assessing the impact of 1.5, 2 and 3 °C global warming.

36

37 **Key Words:** hydrological drought; 1.5, 2 and 3 °C warming levels; CMIP5 models;

38 RCP scenarios; uncertainty analysis.

39

40 **1. Introduction**

41 Global warming has affected both natural and artificial systems across continents,
42 bringing a lot of eco-hydrological crises to many countries (Gitay et al., 2002; Tirado
43 et al., 2010; Thornton et al., 2014). The Intergovernmental Panel on Climate Change
44 (IPCC) Fifth Assessment Report (AR5) concluded that global average surface air
45 temperature increased by 0.61°C in 1986-2005 compared to pre-industrial periods
46 (IPCC, 2014a). In order to mitigate global warming, the Conference of the Parties of
47 the United Nations Framework Convention on Climate Change (UNFCCC)
48 emphasized in the Paris Agreement that the increase in global average temperature
49 should be controlled within 2 °C above preindustrial levels, and further efforts should
50 be made to limit it below 1.5 °C. However, whether the temperature controlling goal
51 can be reached is still unknown, with much difficulty under current emission
52 conditions (Peters et al., 2012). In addition, specific warming level such as 2 °C
53 increase would be too high for many regions and countries (James et al., 2017; Rogelj
54 et al., 2015). Therefore, it is necessary to assess changes in regional hydrological
55 cycle and extremes under 1.5, 2 and even 3 °C global warming.

56 Global warming is mainly caused by greenhouse gases emissions and has a profound
57 influence on hydrosphere and ecosphere (Barnett et al., 2005; Vorosmarty et al., 2000).
58 It alters hydrological cycle both directly (e.g., influences precipitation and
59 evapotranspiration) and indirectly (e.g., influences plant growth and related
60 hydrological processes) at global (Zhu et al., 2016; McVicar et al., 2012) and local
61 scales (Tang et al., 2013; Zheng et al., 2009; Zhang et al., 2008). Besides affecting the

62 mean states of the hydrological conditions, global warming also intensifies
63 hydrological extremes significantly, such as droughts which were regarded as
64 naturally occurring events when water (precipitation, or streamflow, etc.) is
65 significantly below normal over a period of time (Van Loon et al., 2016; Dai, 2011).
66 Among different types of droughts, hydrological droughts focus on the decrease in the
67 availability of water resources, e.g., surface and/or ground water (Lorenzo-Lacruz et
68 al., 2013). Many researchers paid attention to the historical changes, future evolutions
69 and uncertainties, and causing factors for hydrological droughts (Chang et al., 2016;
70 Kormos et al., 2016; Orłowsky and Seneviratne, 2013; Parajka et al., 2016; Perez et
71 al., 2011; Prudhomme et al., 2014; Van Loon and Laaha, 2015; Wanders and Wada,
72 2015; Yuan et al., 2017). Most drought projection studies focused on the future
73 changes over a fixed time period (e.g., late 21st century), but recent studies pointed out
74 the importance on hydrological drought evolution at certain warming levels (Roudier
75 et al., 2016; Marx et al., 2018) given the aim of the Paris Agreement. Moreover, the
76 changes in characteristics (e.g., frequency, duration, severity) of hydrological drought
77 events at specific warming levels received less attention. The projection of these
78 drought characteristics could provide more relevant guidelines for policymakers on
79 implementing adaptation strategies.

80 In the past five decades, a significant decrease in channel discharge was observed in
81 the middle reaches of the Yellow River basin over northern China (Yuan et al., 2018;
82 Zhao et al., 2014), leading to an intensified water resources scarcity in this populated
83 area. In this study, we take a semiarid watershed, the Wudinghe in the middle reaches

84 of the Yellow River basin as a testbed, aiming at solving the following questions: (1)
85 How do hydrological drought characteristics change at different warming levels over
86 the Wudinghe watershed? (2) What are the causes for the hydrological drought change?
87 (3) What are the contributions of uncertainties from different sources (e.g., climate
88 and land surface hydrological models, representative concentration pathways (RCPs)
89 scenarios, and internal variability)?

90 **2. Study area and dataset**

91 In this study, the Wudinghe watershed was chosen for hydrological drought analysis.
92 As one of the largest sub-basins of the Yellow River basin, the Wudinghe watershed is
93 located in the Loess Plateau, and has a drainage area of 30261 km² with Baijiachuan
94 hydrological station as the watershed outlet (Figure 1). It has a semiarid climate with
95 long-term (1956-2010) annual mean precipitation of 356 mm and runoff of 39 mm,
96 resulting in a runoff coefficient of 0.11 (Jiao et al., 2017). Most of the rainfall events
97 are concentrated in summer (June to September) with a large possibility of heavy
98 rains (Mo et al., 2009). Located in the transition zone between cropland/grassland and
99 desert/shrub, the northwest part of the Wudinghe watershed is dominated by sandy
100 soil, while the major soil type for the southeast part is loess soil. During recent
101 decades, the Wudinghe watershed has experienced a significant streamflow decrease
102 (Yuan et al., 2018; Zhao et al., 2014) and suffered from serious water resource
103 scarcity because of climate change, vegetation degradation and human water
104 consumption (Xiao, 2014; Xu, 2011).
105 <Figure 1 here>

106 The Coupled Model Intercomparison Project Phase 5 (CMIP5) general circulation
107 model (GCM) simulations for historical experiments and future projections formed
108 the science basis for the IPCC AR5 reports (IPCC, 2014b; Taylor et al., 2012). In this
109 study, we chose eight CMIP5 GCMs for historical (1961-2005) and future (2006-2099)
110 drought analysis, as they provided daily simulations under all four RCP scenarios (i.e.
111 RCP2.6/4.5/6.0/8.5). Table 1 listed the details of GCMs used in this paper. Because of
112 the deficiency in GCM precipitation and runoff simulations, we used the corrected
113 meteorological forcing data from CMIP5 climate models, to drive a high resolution
114 land surface hydrological model to simulate runoff and streamflow ~~(see Section 3.1~~
115 ~~for details).~~

116 <Table 1 here>

117 All CMIP5 simulations were bias corrected before being used as land surface model
118 input. After interpolating CMIP5 simulations and China Meteorological
119 Administration (CMA) station observations to the same resolution (0.01 degree in this
120 study), a modified correction method (Li et al., 2010) based on widely-used quantile
121 mapping (Wood et al., 2002; Yuan et al., 2015) was applied to adjust CMIP5/ALL
122 historical simulations and CMIP5/RCPs future simulations for each model at each
123 grid cell separately. The bias-corrected daily precipitation and temperature were then
124 further temporally disaggregated to a 6-hours interval based on the diurnal cycle
125 information from CRUNCEP 6-hourly dataset
126 (<https://svn-ccsm-inputdata.cgd.ucar.edu/trunk/inputdata/atm/datm7/>). Other 6-hourly
127 meteorological forcings, i.e., incident solar radiation, air pressure, specific humidity

128 and wind speed, were directly taken from CRUNCEP dataset. [Please see Appendix](#)
129 [Section for details.](#)

130 **3. Land Surface Hydrological Model and Methods**

131 **3.1. Introduction of the CLM-GBHM model**

132 In this study, we chose a newly developed land surface hydrological model,
133 CLM-GBHM, to simulate historical and future streamflow. This model was first
134 developed and applied in the Wudinghe watershed at 0.01 degree (Jiao et al., 2017)
135 and then the Yellow River basin at 0.05 degree resolution (Sheng et al., 2017). By
136 improving surface runoff generation, subsurface runoff scheme, river network-based
137 representation and 1-D kinematic wave river routing processes, CLM-GBHM showed
138 good performances in simulating streamflow, soil moisture content and water table
139 depth (Sheng et al., 2017). Figure 2 demonstrated the structure and main
140 eco-hydrological processes of CLM-GBHM. Model resolution, surface datasets,
141 initial conditions and model parameters were kept consistent with Jiao et al. (2017),
142 except that monthly LAI in 1982 was used for all simulations because of an unknown
143 vegetation condition in the future.

144 <Figure 2 here>

145 **3.2. Determination of years reaching specific warming levels**

146 IPCC AR5 (IPCC, 2014a) reported that global average surface air temperature change
147 between pre-industrial period (1850-1900) and reference period (1986-2005) is 0.61
148 (0.55 to 0.67) °C. Therefore, we took 1986-2005 as the baseline period. Monthly
149 standardized streamflow index (SSI) simulations from CLM-GBHM were compared

150 with the observed records during the baseline period, and the model performed well
151 with a correlative coefficient of 0.53 ($p < 0.01$). Here, “1.5 °C warming level” referred
152 to a global temperature increase of 0.89 ($=1.5-0.61$) °C, “2 °C warming level” referred
153 to an increase of 1.39 ($=2-0.61$) °C, and “3 °C warming level” referred to an increase
154 of 2.39 ($=3-0.61$) °C compared with the baseline, respectively. As large differences
155 existed in temperature simulations among CMIP5 models and RCP scenarios, we
156 applied a widely used time sampling method (James et al., 2017; Mohammed et al.,
157 2017; Marx et al., 2018) to each GCM under each RCP scenario (referred to as
158 GCM/RCP combination hereafter). A 20-years moving window, which has the same
159 length of the baseline period, was used to determine the first period reaching a
160 specific warming level for each combination, with the period median year referred to
161 as the “crossing year”.

162 **3.3. Identification of hydrological drought characteristics**

163 We used a two-step method similar to previous studies (Lorenzo-Lacruz et al., 2013;
164 Ma et al., 2015; Yuan et al., 2017) to extract hydrological drought characteristics in
165 this paper. At the first step, a hydrological drought index named as Standardized
166 Streamflow Index (SSI) was calculated by fitting monthly streamflow using a
167 probabilistic distribution function (Vicente-Serrano et al., 2012; Yuan et al., 2017).
168 Specifically, for each calendar month, streamflow values in that month during
169 baseline period were collected, arranged, and fitted by using a gamma distribution
170 function. Using the same parameters of the fitted gamma distribution, both baseline
171 (1986-2005) and future (2006-2099) streamflow values in that calendar month were

172 standardized to get SSI values. The procedure was repeated for twelve calendar
173 months, four RCP scenarios and eight GCMs separately. The second step was
174 identification and characterization of hydrological drought events by an SSI threshold
175 method (Yuan and Wood, 2013; Lorenzo-Lacruz et al., 2013; Van Loon and Laaha,
176 2015). Here, a threshold of -0.8 was selected, which is equivalent to a dry condition
177 with a probability of 20%. Months with SSI below -0.8 were treated as dry months,
178 and 3 or more continuous dry months were considered as the emergence of a
179 hydrological drought event. To characterize the hydrological drought event, drought
180 duration (months) and severity (sum of the difference between -0.8 and SSI) for a
181 certain drought event were calculated. As future SSI values were all calculated based
182 on historical values, it is important to mention that drought analysis here represented
183 those without adaptation (Samaniego et al., 2018).

184 **3.4. Uncertainty separation**

185 Given large spreads among future projections (including combinations of eight GCMs
186 and four RCP scenarios, as shown in shaded areas in Figure 3), a separation method
187 (Hawkins and Sutton, 2009; Orłowsky and Seneviratne, 2013) was applied to explore
188 uncertainty from three individual sources, i.e., internal variability, climate models and
189 RCPs scenarios. In order to separate internal variability from other two factors with
190 long-term trends, a 4th order polynomial was selected to fit specific time series: the
191 fitting was first carried out during baseline period (1986-2005) to obtain an average i_m
192 as a reference value, and then during future period (2006-2099) to obtain a smooth fit
193 $x_{m,s,t}$. Future projections ($X_{m,s,t}$) were then separated into three parts: reference value

194 (i_m), smooth fit ($x_{m,s,t}$) and residual ($e_{m,s,t}$), and the uncertainties from three sources
195 were then calculated as follows:

$$V = \sum_m \text{var}_{s,t}(e_{m,s,t}) / N_m \quad (1)$$

$$M_t = \sum_s \text{var}_m(x_{m,s,t}) / N_s \quad (2)$$

$$S_t = \text{var}_s(\sum_m x_{m,s,t} / N_m) \quad (3)$$

196 where V , M_t and S_t represent uncertainties from internal variability (which is
197 time-invariant), climate models and RCPs scenarios, N_m and N_s are numbers of
198 climate models and RCPs scenarios, $\text{var}_{s,t}$ denotes the variance across scenarios and
199 time, var_m and var_s are variances across models and scenarios respectively. Finally,
200 uncertainty contributions from each component were calculated as proportions to the
201 sum. In this study, we applied this method to the 20-years moving averaged ensemble
202 time series.

203 4. Results

204 4.1. Changes in hydrometeorology in the past and future

205 We first calculated the trends during both the historical and future periods for
206 basin-averaged annual mean hydrological variables (Table 2 and Figure 3). During
207 1961-2005, there was a significant increasing trend ($p < 0.01$) in observed temperature
208 and a decreasing trend ($p < 0.1$) in observed precipitation, resulted in a decreasing
209 naturalized streamflow ($p < 0.01$) and an increasing hydrological drought frequency
210 ($p < 0.01$). Here, the naturalized streamflow was obtained by adding human water use
211 back to the observed streamflow (Yuan et al., 2017). These historical changes could
212 be captured by hydro-climate model simulations to some extent, although both the

213 warming and drying trends were underestimated (Table 2). Ensemble monthly SSI
214 series from GCM driven model simulations were also compared with offline results
215 (CRUNCEP driven) during historical period, resulted in a correlative coefficient of
216 0.47 ($p < 0.01$). During 2006-2099, four variables show consistent changing trends
217 across RCPs scenarios, but with different magnitudes (Table 2). Future temperature
218 and precipitation will increase, resulting in an increasing streamflow and decreasing
219 hydrological drought frequency. Unlike temperature trends that increase from RCP2.6
220 to RCP8.5 (which indicates different radiative forcings), precipitation trend under
221 RCP6.0 is smaller than that under RCP4.5, suggesting a nonlinear response of
222 regional water cycle to the increase in radiative forcings. As a result, RCP6.0 shows
223 the smallest increasing rate in streamflow and decreasing rate in drought frequency.

224 <Table 2 here>

225 More details could be found in Figure 3 when focusing on dynamic changes in the
226 history and future. Figure 3a shows that the differences in temperature among RCPs
227 are negligible until 2030s when RCP8.5 starts to outclass other scenarios, and the
228 others begin to diverge in the far future (2060s-2080s). In contrast, differences in
229 future precipitation are small throughout the 21st century, except that RCP8.5 scenario
230 becomes larger after 2080s (Figure 3b). As comprehensive outcomes of climate and
231 eco-hydrological factors, a clear decrease-increase pattern in streamflow and an
232 increase-decrease trend in hydrological drought frequency are found (Figure 3c and
233 3d). However, differences among RCPs are not discernible. Figures 3b-3d also show
234 that the differences in water-related variables among climate models are very large.

235 <Figure 3 here>

236 Using the time-sampling method mentioned in Section 3.2, first 20-year periods with
237 mean temperature increasing across 1.5, 2 and 3 °C warming levels for each
238 GCM/RCP combination were identified and listed in Table 3. To demonstrate the
239 overall situation for a specific warming level, we chose median year among GCMs as
240 model ensemble for each RCP scenario, and median year among all GCMs and RCPs
241 as total ensemble. GCM/RCP combinations not reaching specific warming level were
242 marked as “NR” in Table 3 and were not considered when calculating ensemble year.

243 <Table 3 here>

244 As listed in Table 3, crossing years for most GCM/RCP combinations reaching 1.5 °C
245 warming level are before 2032 except for GFDL-ESM2M and MRI-CGCM3. Model
246 ensemble years for different RCP scenarios have small differences, and total ensemble
247 year for all GCMs and RCPs is 2025, indicating that 1.5 °C warming level would be
248 reached within 2015-2034. As for 2 and 3 °C warming level, the total ensemble year is
249 2042 and 2070, respectively. There are large differences in crossing years among
250 different GCMs, ranging from 2016 to 2075 for 1.5 °C, 2030 to 2076 for 2 °C, and
251 2051 to 2086 for 3 °C. Generally, three global warming thresholds would be reached
252 first under RCP8.5 and last under RCP6.0 scenario. All GCMs will not reach 3 °C
253 warming level under RCP2.6, while under other RCP scenarios this temperature
254 increase would probably be reached around 2073 or even as early as 2050s.

255 **4.2. Hydrological changes at 1.5, 2 and 3 °C warming levels**

256 After identifying the time periods reaching specific warming levels, we collected

257 precipitation and runoff data within these periods (different among GCM/RCP
258 combinations), and calculated their relative changes compared to the baseline period
259 (1986-2005). Figure 4 shows the spatial pattern of relative changes in model ensemble
260 mean precipitation of these time periods, except for the period under RCP2.6 at 3 °C
261 warming level during which no sample exists. Results indicate that precipitation will
262 increase at all warming levels and all RCP scenarios, while differences exist in spatial
263 patterns. The ensemble mean precipitation increases by 8.0%, 9.1% and 18.0% at 1.5,
264 2 and 3 °C warming levels for all RCP scenarios respectively, indicating larger
265 increase in precipitation when warming level increases. For each warming level,
266 precipitation changes among all RCP scenarios are quite close except for RCP6.0 at
267 3 °C warming level. Larger precipitation increases generally occur in the south and
268 southwest parts which are upstream regions of the Wudinghe watershed.

269 <Figure 4 here>

270 The watershed-mean runoff increases by 26.7%, 18.7% and 44.5% at each warming
271 level respectively, which are larger than those of precipitation because of nonlinear
272 hydrological response (Figure 5). For all warming levels, RCP8.5 shows greatest
273 runoff increase and RCP2.6/6.0 the lowest. Small or negative changes in runoff
274 emerge in the north and southeast regions under RCP2.6/4.5/6.0 scenarios (Figure 5),
275 where precipitation increases the least (Figure 4). Besides, runoff changes are also
276 closely linked to watershed river networks, with large increase in the south and
277 middle parts (upper and middle reaches) and small increase or even decrease in the
278 southeast and northeast parts (lower reaches), showing the redistribution effect of

279 surface topography and soil property.

280 <Figure 5 here>

281 Figure 6 shows the characteristics of hydrological droughts during baseline period and
282 the periods reaching all warming levels. The number of hydrological drought events
283 averaged among all RCP scenarios and climate models is 7 in the baseline period, and
284 it drops to 6.2 (-11% relative to baseline, the same below) at 1.5 °C, 5.2 (-26%) at
285 2 °C and 5.4 (-23%) at 3 °C warming levels (Figure 6a). However, hydrological
286 drought duration increases from 5 months at baseline to 6.5 (+30%), 5.9 (+18%) and 6
287 months (+20%) at 1.5, 2 and 3 °C warming levels, respectively. Drought severity
288 increases dramatically from 1.9 at baseline to 5.4 (+184%) at 1.5 °C warming level,
289 and then drops to 4.1 (+116%) at 2 °C warming level and rebounds to 5.4 (+184%) at
290 3 °C warming level (Figure 6a). These results indicate that although precipitation and
291 runoff increase, the Wudinghe watershed would suffer from more severe hydrological
292 events in the near future at 1.5 °C warming level. The severity could be alleviated in
293 time periods reaching 2 °C warming level, with more precipitation occurring over the
294 watershed.

295 <Figure 6 here>

296 The analysis on individual scenarios suggests a similar conclusion (Figures 6b-6e).
297 Drought amount and severity increase generally when radiative forcing increases. The
298 least changes in drought severity are found under RCP4.5 scenario while the largest
299 changes are under RCP6.0 scenario. Higher warming levels could lead to more
300 moderate drought events under low emission scenarios (RCP2.6/4.5) because of more

301 precipitation in the near future, while high emissions (RCP6.0/8.5) would increase the
302 risk of hydrological drought significantly.

303 **5. Discussion**

304 To explore the reason for less frequent but more severe hydrological droughts, we
305 compared the differences in monthly precipitation, evapotranspiration,
306 total/surface/sub-surface runoff and streamflow between the baseline period and
307 periods reaching 1.5, 2 and 3 °C warming levels. Standardized indices for these
308 hydrological variables were used to remove seasonality from monthly time series, and
309 mean values and variabilities of these indices were chosen as indicators.

310 <Figure 7 here>

311 Figure 7 shows that mean values increase as temperature increases for all standardized
312 hydrological indices, showing a wetter hydroclimate in the future with more
313 precipitation, evapotranspiration, runoff and streamflow (Figure 7a). However,
314 variabilities for the standardized indices in the future are much higher than those
315 during baseline period, indicating larger fluctuations and higher chance for extreme
316 droughts/floods at all warming levels (Figure 7b). For extreme drought events (with
317 an SSI < -1.3, representing a dry condition with a probability of 10%), the ensemble
318 mean amount of drought events are 4.3, 3.1 and 3.7 at 1.5, 2 and 3 °C warming levels,
319 which are much larger than the baseline period with 0.9 (not shown). Focusing on the
320 gaps between baseline and future periods, it is clear that the differences in both
321 evapotranspiration and runoff are larger than those of precipitation for mean values
322 and standard deviations, suggesting the water redistribution through complicated

323 hydrological processes. The increase in mean value of runoff and consequently
324 streamflow mainly comes from the increase in subsurface runoff. As hydrological
325 drought defined in this paper is based on monthly SSI series, increases in both mean
326 value and variability in precipitation and evapotranspiration indicate a period with
327 less frequent but more severe hydrological drought events.

328 Another issue is the reliability of results considering large differences among CMIP5
329 models. Figure 8 shows the uncertainty fractions contributed from internal variability,
330 climate models and RCPs scenarios based on multi-model and multi-scenario
331 ensemble projections of temperature, precipitation, streamflow and drought frequency.
332 Uncertainty in temperature projection is mainly contributed by climate models before
333 2052, and it is then taken over by RCPs scenarios. Internal variability contributes to
334 less than 1.5% of the uncertainty for the temperature projection (Figure 8a). For
335 precipitation projection, climate models account for a large proportion of uncertainty
336 throughout the century. The internal variability contributes to larger uncertainty than
337 RCPs scenarios until the second half of the 21st century (Figure 8b). Similar to
338 precipitation, major source of uncertainty for the projections of streamflow and
339 hydrological drought frequency comes from climate and land surface hydrological
340 models, while the impacts of both internal variability and RCP scenarios are further
341 weakened (Figures 8c-8d).

342 <Figure 8 here>

343 Generally for all variables except temperature, Model-GCMs and land surface
344 hydrological model accounts for over 80% of total uncertainties, while internal

345 variability contributes to a comparable or larger proportion than RCPs scenarios, ~~for~~
346 ~~all variables except temperature (see Table 4). RCPs scenario uncertainty accounts for~~
347 ~~14.3% of temperature uncertainty at 1.5 °C warming level with this proportion~~
348 ~~increasing to 33% (63.7%) at 2 °C (3 °C) warming level, while its contribution to~~
349 ~~precipitation uncertainty remains less than 10%.~~ RCPs scenario only contributes to
350 around 5% of the uncertainties in the projections of streamflow and hydrological
351 drought frequency. These results indicate that the improvement in GCM simulated
352 precipitation would largely narrow the uncertainties for future projections of
353 hydrological droughts. Besides, previous studies (Marx et al., 2018; Samaniego et al.,
354 2018) have shown that uncertainties contributed from land surface hydrological
355 models can be comparable to that from GCMs, indicating the importance of
356 introducing multiple land surface hydrological models into the analysis of uncertainty,
357 and the significance of exploring more suitable methods in further studies.

358 <Table 4 here>

359 There are also some issues for further investigations. As shown in Figure 3, GCM
360 historical simulations underestimates the increasing trend in temperature and
361 decreasing trend in precipitation, and results in underestimations of hydrological
362 drying trends. Although the quantile mapping method used in this study is able to
363 remove the biases in GCM simulations (e.g., mean value, variance), the
364 underestimation of trends could not be corrected. An alternative method is to use
365 regional climate models for dynamical downscaling, which would be useful if
366 regional forcings (e.g., topography, land use change, aerosol emission) are strong.

367 Another issue is about the spatially varied warming rates. IPCC AR5 reported (IPCC,
368 2014c) that global warming for the last 20 years compared to pre-industrial are
369 0.3-1.7 °C (RCP2.6), 1.1-2.6 °C (RCP4.5), 1.4-3.1 °C (RCP6.0), 2.6-4.8 °C (RCP8.5).
370 However, temperature increases vary a lot for different regions. For instance,
371 temperature rises faster in high-altitude (Kraaijenbrink et al., 2017) and polar regions
372 (Bromwich et al., 2013), where the rate of regional warming could be three times of
373 global warming. Actually, reaching periods for regional warming thresholds in the
374 Wudinghe watershed are earlier than the global ones (not shown here), which suggest
375 that the regional warming would be more severe at specific global warming levels.

376 **6. Conclusions**

377 In this paper, we bias-corrected future projections of meteorological forcings from
378 eight CMIP5 GCM simulations under four RCP scenarios to drive a newly developed
379 land surface hydrological model, CLM-GBHM, to project changes in streamflow and
380 hydrological drought characteristics over the Wudinghe watershed. After determining
381 the time periods reaching 1.5, 2 and 3 °C global warming levels for each GCM/RCP
382 combination, we focused on the changes in regional hydrological drought
383 characteristics at all warming levels. Moreover, projection uncertainties from different
384 sources were separated and analyzed. Main conclusions are listed as follows:

385 (1) With CMIP5 GCM simulations as forcing data, the model ensemble mean hindcast
386 can reproduce the significant decreasing trend of streamflow and increasing trend of
387 hydrological drought frequency in historical period (1961-2005), but the drying trend
388 is underestimated because of GCM uncertainties. Streamflow increases and

389 hydrological drought frequency decreases in the future under all RCP scenarios.

390 (2) The time periods reaching 1.5, 2 and 3 °C warming levels over the Wudinghe
391 watershed are 2015-2034, 2032-2051 and 2060-2079, respectively. There are large
392 differences in results among different GCMs, while different RCP scenarios show
393 consistence in reaching periods with RCP8.5 the earliest and RCP6.0 the latest.

394 (3) Precipitation increases under all RCP scenarios at all warming levels (8%, 9% and
395 18%), while differences exist in spatial patterns. Runoff has larger relative change
396 rates (27%, 19% and 44%), with larger increases of runoff occurred in the upper and
397 middle reaches and less increases or even decreases emerged in the lower reaches,
398 indicating a complex spatial distribution in hydrological droughts.

399 (4) As a result of increasing mean values and variability for precipitation,
400 evapotranspiration and runoff, hydrological drought frequency drops by 11%-26% at
401 all warming levels compared to the baseline period, while hydrological drought
402 severity rises dramatically by 116%-184%. This indicates that the Wudinghe
403 watershed would suffer more severe hydrological drought events in the future,
404 especially under RCP6.0 and RCP8.5 scenarios.

405 (5) The main uncertainty sources vary among hydrological variables. Most
406 uncertainties are from climate and land surface models, especially for precipitation. At
407 all warming levels, models contribute to over 80% of total uncertainties, while
408 internal variability contributes to a comparable proportion of uncertainties to RCPs
409 scenarios for precipitation, streamflow and hydrological drought frequency.

410

411 **Acknowledgements**

412 We would like to thank the editor and two anonymous reviewers for their helpful
413 comments. This research was supported by National Key R&D Program of China
414 (2018YFA0606002), [Strategic Priority Research Program of Chinese Academy of](#)
415 [Sciences \(XDA20020201\)](#), National Natural Science Foundation of China (91547103),
416 and the Startup Foundation for Introducing Talent of NUIST. Daily precipitation and
417 temperature simulated by CMIP5 models were provided by the World Climate
418 Research Programme's Working Group on Coupled Modeling
419 (<https://esgf-data.dkrz.de/search/cmip5-dkrz>). We thank Prof. Dawen Yang and Prof.
420 Huimin Lei for the implementation of the CLM-GBHM land surface hydrological
421 model.

423 **Appendix: Details of Processing Climate Forcings**

424 The land surface hydrological model CLM-GBHM requires a list of input climate
425 forcings, i.e. precipitation, near surface air temperature, incident solar radiation, air
426 pressure, specific humidity and wind speed. These variables were generated from
427 three datasets in this study: CMIP5 daily simulations during both historical
428 (1961-2005) and future (2006-2099) periods, CRUNCEP 6-hourly dataset during
429 1959-2005, and China Meteorological Administration (CMA) daily station
430 observations during 1961-2005. All datasets were firstly regridded to the same
431 resolution (0.01 degree) by using bilinear interpolation method for further processing.
432 After spatial interpolation, daily precipitation and temperature from CMIP5

带格式的: paper_一级标题, 行距:
单倍行距

带格式的: 英语(美国)

433 simulations were adjusted to remove their monthly biases compared to CMA
 434 observations, by applying a correction method to each model at each grid cell
 435 separately. This method modified the widely used quantile-mapping method (CDFm)
 436 and processed historical and future timeseries in different ways. For historical period,
 437 bias-corrected monthly variable x (i.e., precipitation or temperature) was calculated
 438 based on CDFm:

$$\underline{x_{sim, his, corrected} = F_{obs, his}^{-1}(F_{sim, his}(x_{sim, his, biased}))} \quad (A1)$$

439 where F is cumulative distribution function of variable x , subscripts $sim, obs, his,$
 440 $biased, corrected$ represent simulated value, observed value, historical period, value
 441 with bias and value after bias correction at monthly scale, respectively. The basic
 442 assumption of CDFm is that the climate distribution does not change much over time,
 443 however, this is invalid considering intense global warming in the future. Therefore,
 444 an equidistant CDF matching method (EDCDFm; Li et al., 2010) was applied for
 445 future projections, which assumes that the difference between simulated and observed
 446 values remains the same over time:

$$\underline{x_{sim, fut, corrected} = x_{sim, fut, biased} + F_{obs, his}^{-1}(F_{sim, fut}(x_{sim, fut, biased})) - F_{sim, his}^{-1}(F_{sim, fut}(x_{sim, fut, biased}))} \quad (A2)$$

447 where subscript fut represents future period. After bias correction at monthly scale,
 448 new daily precipitation (temperature) series were generated based on the ratio
 449 (difference) between the new and old CMIP5 simulated monthly means:

$$\underline{P_{d, corrected} = (P_{m, corrected} / P_{m, biased}) \cdot P_{d, biased}} \quad (A3)$$

$$\underline{T_{d, corrected} = (T_{m, corrected} - T_{m, biased}) + T_{d, biased}} \quad (A4)$$

带格式的: 字体: 倾斜

带格式的: 字体: 倾斜

带格式的: 字体: 倾斜

带格式的: 字体: 倾斜

带格式的: 字体: 倾斜

带格式的: 字体: 倾斜

带格式的: 字体: 倾斜

带格式的: 字体: 倾斜

带格式的: 降低量 17 磅

带格式的: 字体: 倾斜

带格式的: 字体: 倾斜

带格式的: 字体: 倾斜

带格式的: 字体: 倾斜

带格式的: 字体: 倾斜

450 where P and T represent precipitation and temperature, subscripts d and m represent
451 daily value and corresponding monthly mean, respectively.

452 In order to temporally disaggregate daily temperature and precipitation to a 6-hours
453 interval during both historical and future periods, the diurnal cycle information from
454 CRUNCEP dataset was introduced. By looping the CRUNCEP data during 1959-2005
455 (47 years) twice, we could also generate “future data” (2006-2099, 94 years). By
456 using the same disaggregation method that downscales variables from monthly to
457 daily, temporal downscaling from daily to 6-hourly scales was achieved:

$$P_{6h,corrected} = (P_{d,corrected} / P_{d,CRUNCEP}) \cdot P_{6h,CRUNCEP} \quad (A5)$$

$$T_{6h,corrected} = (T_{d,corrected} - T_{d,CRUNCEP}) + T_{6h,CRUNCEP} \quad (A6)$$

带格式的: 字体: 倾斜

458 where subscript $6h$ represents 6-hourly values. It should be mentioned that only
459 precipitation and temperature have been used from CMIP5 models, with other climate
460 forcing variables (i.e., incident solar radiation, air pressure, specific humidity and
461 wind speed series) directly taken from CRUNCEP dataset. Whether physical
462 consistency among all climate forcing variables was maintained or not by simply
463 introducing CRUNCEP dataset was not considered in this study, and it is unclear how
464 the climate change signals by GCMs might be affected by using CRUNCEP data for a
465 majority of forcing variables. Although resampling methods (e.g., Schaake Shuffle)
466 that are widely used in temporal downscaling for seasonal forecasting might result in
467 more consistent forcing variables, whether such consistency (e.g.,
468 temperature-humidity relationship) holds for future projection given the changing
469 climate is unknown. More sophisticated downscaling techniques (either statistical or

470 | dynamical) are needed for further studies.

471

472

473 **References**

- 474 Barnett, T. P., Adam, J. C., and Lettenmaier, D. P.: Potential impacts of a warming
475 climate on water availability in snow-dominated regions, *Nature*, 438, 303-309,
476 doi:10.1038/nature04141, 2005.
- 477 Bromwich, D. H., Nicolas, J. P., Monaghan, A. J., Lazzara, M. A., Keller, L. M.,
478 Weidner, G. A., and Wilson, A. B.: Central West Antarctica among the most
479 rapidly warming regions on Earth, *Nat Geosci*, 6, 139-145,
480 doi:10.1038/Ngeo1671, 2013.
- 481 Chang, J., Li, Y., Wang, Y., and Yuan, M.: Copula-based drought risk assessment
482 combined with an integrated index in the Wei River Basin, China, *Journal of*
483 *Hydrology*, 540, 824-834, doi:10.1016/j.jhydrol.2016.06.064, 2016.
- 484 Dai, A. G.: Drought under global warming: a review, *Wires Clim Change*, 2, 45-65,
485 doi:10.1002/wcc.81, 2011.
- 486 Gitay, H., Suárez, A., Watson, R. T., and Dokken, D. J.: Climate change and
487 biodiversity, IPCC Technical Paper V, 2002.
- 488 Hawkins, E., and Sutton, R.: The Potential to Narrow Uncertainty in Regional
489 Climate Predictions, *B Am Meteorol Soc*, 90, 1095-+,
490 doi:10.1175/2009bams2607.1, 2009.
- 491 IPCC: Climate Change 2013 - The Physical Science Basis, Cambridge University
492 Press, Cambridge, United Kingdom and New York, NY, USA, 1535 pp., 2014a.
- 493 IPCC: Summary for Policymakers, in: Climate Change 2013 - The Physical Science
494 Basis, edited by: Stocker, T. F., Qin, D., Plattner, G.-K., Tignor, M., Allen, S. K.,
495 Boschung, J., Nauels, A., Xia, Y., Bex, V., and Midgley, P. M., Cambridge
496 University Press, Cambridge, United Kingdom and New York, NY, USA, 1-30,
497 2014b.
- 498 IPCC: Long-term Climate Change: Projections, Commitments and Irreversibility, in:
499 Climate Change 2013 - The Physical Science Basis, edited by: Stocker, T. F.,
500 Qin, D., Plattner, G.-K., Tignor, M., Allen, S. K., Boschung, J., Nauels, A., Xia,
501 Y., Bex, V., and Midgley, P. M., Cambridge University Press, Cambridge,

502 United Kingdom and New York, NY, USA, 1029-1136, 2014c.

503 James, R., Washington, R., Schleussner, C. F., Rogelj, J., and Conway, D.:
504 Characterizing half-a-degree difference: a review of methods for identifying
505 regional climate responses to global warming targets, *Wires Clim Change*, 8,
506 doi:10.1002/wcc.457, 2017.

507 Jiao, Y., Lei, H. M., Yang, D. W., Huang, M. Y., Liu, D. F., and Yuan, X.: Impact of
508 vegetation dynamics on hydrological processes in a semi-arid basin by using a
509 land surface-hydrology coupled model, *Journal of Hydrology*, 551, 116-131,
510 doi:10.1016/j.jhydrol.2017.05.060, 2017.

511 Kormos, P. R., Luce, C. H., Wenger, S. J., and Berghuijs, W. R.: Trends and
512 sensitivities of low streamflow extremes to discharge timing and magnitude in
513 Pacific Northwest mountain streams, *Water Resour Res*, 52, 4990-5007,
514 doi:10.1002/2015wr018125, 2016.

515 Kraaijenbrink, P. D. A., Bierkens, M. F. P., Lutz, A. F., and Immerzeel, W. W.:
516 Impact of a global temperature rise of 1.5 degrees Celsius on Asia's glaciers,
517 *Nature*, 549, 257-+, doi:10.1038/nature23878, 2017.

518 Li, H. B., Sheffield, J., and Wood, E. F.: Bias correction of monthly precipitation and
519 temperature fields from Intergovernmental Panel on Climate Change AR4
520 models using equidistant quantile matching, *J Geophys Res-Atmos*, 115,
521 doi:10.1029/2009jd012882, 2010.

522 Lorenzo-Lacruz, J., Moran-Tejeda, E., Vicente-Serrano, S. M., and Lopez-Moreno, J.
523 I.: Streamflow droughts in the Iberian Peninsula between 1945 and 2005: spatial
524 and temporal patterns, *Hydrology and Earth System Sciences*, 17, 119-134,
525 doi:10.5194/hess-17-119-2013, 2013.

526 Ma, F., Yuan, X., and Ye, A. Z.: Seasonal drought predictability and forecast skill
527 over China, *J Geophys Res-Atmos*, 120, 8264-8275, doi:10.1002/2015jd023185,
528 2015.

529 Marx, A., Kumar, R., Thober, S., Rakovec, O., Wanders, N., Zink, M., Wood, E. F.,
530 Pan, M., Sheffield, J., and Samaniego, L.: Climate change alters low flows in

531 Europe under global warming of 1.5, 2, and 3 degrees C, *Hydrology and Earth*
532 *System Sciences*, 22, 1017-1032, doi:10.5194/hess-22-1017-2018, 2018.

533 McVicar, T. R., Roderick, M. L., Donohue, R. J., Li, L. T., Van Niel, T. G., Thomas,
534 A., Grieser, J., Jhajharia, D., Himri, Y., Mahowald, N. M., Mescherskaya, A. V.,
535 Kruger, A. C., Rehman, S., and Dinpashoh, Y.: Global review and synthesis of
536 trends in observed terrestrial near-surface wind speeds: Implications for
537 evaporation, *Journal of Hydrology*, 416, 182-205,
538 doi:10.1016/j.jhydrol.2011.10.024, 2012.

539 Mo, X. G., Liu, S. X., Chen, D., Lin, Z. H., Guo, R. P., and Wang, K.: Grid-size
540 effects on estimation of evapotranspiration and gross primary production over a
541 large Loess Plateau basin, China, *Hydrolog Sci J*, 54, 160-173,
542 doi:10.1623/hysj.54.1.160, 2009.

543 Mohammed, K., Islam, A. S., Islam, G. M. T., Alfieri, L., Bala, S. K., and Khan, M. J.
544 U.: Extreme flows and water availability of the Brahmaputra River under 1.5 and
545 2 A degrees C global warming scenarios, *Climatic Change*, 145, 159-175,
546 doi:10.1007/s10584-017-2073-2, 2017.

547 Orłowsky, B., and Seneviratne, S. I.: Elusive drought: uncertainty in observed trends
548 and short- and long-term CMIP5 projections, *Hydrology and Earth System*
549 *Sciences*, 17, 1765-1781, doi:10.5194/hess-17-1765-2013, 2013.

550 Parajka, J., Blaschke, A. P., Bloeschl, G., Haslinger, K., Hepp, G., Laaha, G.,
551 Schoener, W., Trautvetter, H., Viglione, A., and Zessner, M.: Uncertainty
552 contributions to low-flow projections in Austria, *Hydrology and Earth System*
553 *Sciences*, 20, 2085-2101, doi:10.5194/hess-20-2085-2016, 2016.

554 Perez, G. A. C., van Huijgevoort, M. H. J., Voss, F., and van Lanen, H. A. J.: On the
555 spatio-temporal analysis of hydrological droughts from global hydrological
556 models, *Hydrology and Earth System Sciences*, 15, 2963-2978,
557 doi:10.5194/hess-15-2963-2011, 2011.

558 Peters, G. P., Andrew, R. M., Boden, T., Canadell, J. G., Ciais, P., Le Quéré, C.,
559 Marland, G., Raupach, M. R., and Wilson, C.: The challenge to keep global

560 warming below 2 C, *Nat Clim Change*, 3, 4, 2012.

561 Prudhomme, C., Giuntoli, I., Robinson, E. L., Clark, D. B., Arnell, N. W., Dankers,
562 R., Fekete, B. M., Franssen, W., Gerten, D., Gosling, S. N., Hagemann, S.,
563 Hannah, D. M., Kim, H., Masaki, Y., Satoh, Y., Stacke, T., Wada, Y., and
564 Wissler, D.: Hydrological droughts in the 21st century, hotspots and uncertainties
565 from a global multimodel ensemble experiment, *Proceedings of the National*
566 *Academy of Sciences*, 111, 3262-3267, doi:10.1073/pnas.1222473110, 2014.

567 Rogelj, J., Luderer, G., Pietzcker, R. C., Kriegler, E., Schaeffer, M., Krey, V., and
568 Riahi, K.: Energy system transformations for limiting end-of-century warming to
569 below 1.5 degrees C, *Nat Clim Change*, 5, 519+, doi:10.1038/nclimate2572,
570 2015.

571 Roudier, P., Andersson, J. C. M., Donnelly, C., Feyen, L., Greuell, W., and Ludwig,
572 F.: Projections of future floods and hydrological droughts in Europe under a+2
573 degrees C global warming, *Climatic Change*, 135, 341-355,
574 doi:10.1007/s10584-015-1570-4, 2016.

575 Samaniego, L., Thober, S., Kumar, R., Wanders, N., Rakovec, O., Pan, M., Zink, M.,
576 Sheffield, J., Wood, E., and Marx, A.: Anthropogenic warming exacerbates
577 European soil moisture droughts, *Nat Clim Change*, 8, 421, 2018, doi:
578 10.1038/s41558-018-0138-5

579 Sheng, M. Y., Lei, H. M., Jiao, Y., and Yang, D. W.: Evaluation of the Runoff and
580 River Routing Schemes in the Community Land Model of the Yellow River
581 Basin, *J Adv Model Earth Sy*, 9, 2993-3018, doi:10.1002/2017ms001026, 2017.

582 Tang, Y., Tang, Q., Tian, F., Zhang, Z., and Liu, G.: Responses of natural runoff to
583 recent climatic variations in the Yellow River basin, China, *Hydrology and Earth*
584 *System Sciences*, 17, 4471-4480, doi: 10.5194/hess-17-4471-2013, 2013.

585 Taylor, K. E., Stouffer, R. J., and Meehl, G. A.: An Overview of Cmp5 and the
586 Experiment Design, *B Am Meteorol Soc*, 93, 485-498,
587 doi:10.1175/Bams-D-11-00094.1, 2012.

588 Thornton, P. K., Ericksen, P. J., Herrero, M., and Challinor, A. J.: Climate variability

589 and vulnerability to climate change: a review, *Global Change Biol*, 20,
590 3313-3328, doi:10.1111/gcb.12581, 2014.

591 Tirado, M. C., Clarke, R., Jaykus, L. A., McQuatters-Gollop, A., and Franke, J. M.:
592 Climate change and food safety: A review, *Food Res Int*, 43, 1745-1765,
593 doi:10.1016/j.foodres.2010.07.003, 2010.

594 Van Loon, A. F., and Laaha, G.: Hydrological drought severity explained by climate
595 and catchment characteristics, *Journal of Hydrology*, 526, 3-14,
596 doi:10.1016/j.jhydrol.2014.10.059, 2015.

597 Van Loon, A. F., Stahl, K., Di Baldassarre, G., Clark, J., Rangelcroft, S., Wanders, N.,
598 Gleeson, T., Van Dijk, A. I. J. M., Tallaksen, L. M., Hannaford, J., Uijlenhoet, R.,
599 Teuling, A. J., Hannah, D. M., Sheffield, J., Svoboda, M., Verbeiren, B.,
600 Wagener, T., and Van Lanen, H. A. J.: Drought in a human-modified world:
601 reframing drought definitions, understanding, and analysis approaches,
602 *Hydrology and Earth System Sciences*, 20, 3631-3650,
603 doi:10.5194/hess-20-3631-2016, 2016.

604 Vicente-Serrano, S. M., Lopez-Moreno, J. I., Begueria, S., Lorenzo-Lacruz, J.,
605 Azorin-Molina, C., and Moran-Tejeda, E.: Accurate Computation of a
606 Streamflow Drought Index, *J Hydrol Eng*, 17, 318-332,
607 doi:10.1061/(Asce)He.1943-5584.0000433, 2012.

608 Vorosmarty, C. J., Green, P., Salisbury, J., and Lammers, R. B.: Global water
609 resources: Vulnerability from climate change and population growth, *Science*,
610 289, 284-288, doi:10.1126/science.289.5477.284, 2000.

611 Wanders, N., and Wada, Y.: Human and climate impacts on the 21st century
612 hydrological drought, *Journal of Hydrology*, 526, 208-220,
613 doi:10.1016/j.jhydrol.2014.10.047, 2015.

614 Wood, A. W., Maurer, E. P., Kumar, A., and Lettenmaier, D. P.: Long-range
615 experimental hydrologic forecasting for the eastern United States, *J Geophys*
616 *Res-Atmos*, 107, doi:10.1029/2001jd000659, 2002.

617 Xiao, J. F.: Satellite evidence for significant biophysical consequences of the "Grain

618 for Green" Program on the Loess Plateau in China, *J Geophys Res-Bioge*, 119,
619 2261-2275, doi:10.1002/2014jg002820, 2014.

620 Xu, J. X.: Variation in annual runoff of the Wudinghe River as influenced by climate
621 change and human activity, *Quatern Int*, 244, 230-237,
622 doi:10.1016/j.quaint.2010.09.014, 2011.

623 Yuan, X., and Wood, E. F.: Multimodel seasonal forecasting of global drought onset,
624 *Geophys Res Lett*, 40, 4900-4905, doi:10.1002/grl.50949, 2013.

625 Yuan, X., Roundy, J. K., Wood, E. F., and Sheffield, J.: Seasonal forecasting of
626 global hydrologic extremes: system development and evaluation over GEWEX
627 basins, *B Am Meteorol Soc*, 96, 1895-1912, doi:10.1175/BAMS-D-14-00003.1,
628 2015.

629 Yuan, X., Zhang, M., Wang, L. Y., and Zhou, T.: Understanding and seasonal
630 forecasting of hydrological drought in the Anthropocene, *Hydrology and Earth
631 System Sciences*, 21, 5477-5492, doi:10.5194/hess-21-5477-2017, 2017.

632 Yuan, X., Y. Jiao, D. Yang, and H. Lei: Reconciling the attribution of changes in
633 streamflow extremes from a hydroclimate perspective, *Water Resour Res*,
634 doi:10.1029/2018WR022714, 2018

635 Zhang, X. P., Zhang, L., Zhao, J., Rustomji, P., and Hairsine, P.: Responses of
636 streamflow to changes in climate and land use/cover in the Loess Plateau, China,
637 *Water Resour Res*, 44, doi:10.1029/2007wr006711, 2008.

638 Zhao, G. J., Tian, P., Mu, X. M., Jiao, J. Y., Wang, F., and Gao, P.: Quantifying the
639 impact of climate variability and human activities on streamflow in the middle
640 reaches of the Yellow River basin, China, *Journal of Hydrology*, 519, 387-398,
641 doi:10.1016/j.jhydrol.2014.07.014, 2014.

642 Zheng, H. X., Zhang, L., Zhu, R. R., Liu, C. M., Sato, Y., and Fukushima, Y.:
643 Responses of streamflow to climate and land surface change in the headwaters of
644 the Yellow River Basin, *Water Resour Res*, 45, doi:10.1029/2007wr006665,
645 2009.

646 Zhu, Z. C., Piao, S. L., Myneni, R. B., Huang, M. T., Zeng, Z. Z., Canadell, J. G.,

647 Ciais, P., Sitch, S., Friedlingstein, P., Armeth, A., Cao, C. X., Cheng, L., Kato, E.,
648 Koven, C., Li, Y., Lian, X., Liu, Y. W., Liu, R. G., Mao, J. F., Pan, Y. Z., Peng,
649 S. S., Penuelas, J., Poulter, B., Pugh, T. A. M., Stocker, B. D., Viovy, N., Wang,
650 X. H., Wang, Y. P., Xiao, Z. Q., Yang, H., Zaehle, S., and Zeng, N.: Greening of
651 the Earth and its drivers, *Nat Clim Change*, 6, 791-795,
652 doi:10.1038/nclimate3004, 2016.

653 **Figure Captions**

654 **Figure 1.** Location, elevation and river networks for the Wudinghe watershed.

655 **Figure 2.** Structure and main eco-hydrological processes for the land surface
656 hydrological model CLM-GBHM. (modified from Jiao et al., 2017)

657 **Figure 3.** Historical (ALL) and future (RCP2.6/4.5/6.0/8.5) time series of
658 standardized annual mean (a) temperature, (b) precipitation and (c) streamflow, and (d)
659 the time series of hydrological drought frequency (drought months for each year) over
660 the Wudinghe watershed. Shaded areas indicate the ranges between maximum and
661 minimum values among CMIP5/CLM-GBHM model simulations. ALL represents
662 historical simulations with both anthropogenic and natural forcings,
663 RCP2.6/4.5/6.0/8.5 represent four representative concentration pathways from lower
664 to higher emission scenarios.

665 **Figure 4.** Spatial pattern of relative changes in multi-model ensemble mean
666 precipitation at 1.5, 2 and 3 °C warming levels compared to the baseline period
667 (1986-2005). The percentages in the upper-right corners of each panel are the
668 watershed-mean changes for different RCP scenarios, and the percentages in the top
669 brackets are the mean values from four RCP scenarios.

670 **Figure 5.** The same as **Figure 4**, but for the spatial patterns of runoff changes.

671 **Figure 6.** Comparison of the characteristics (amount (number of drought events per
672 20 years), duration (months) and severity) averaged among climate models and RCP
673 scenarios for hydrological drought events during the baseline period (1986-2005) and
674 the periods reaching 1.5, 2 and 3 °C warming levels. Black lines indicate 5%-95%

675 confidence intervals.

676 **Figure 7.** Comparison of (a) mean values and (b) standard deviations for hydrological
677 indices averaged among climate models and RCP scenarios during the baseline period
678 (1986-2005) and the periods reaching 1.5, 2 and 3 °C warming levels. SPI, SEI, SRI,
679 SSRI, SBI, SSI represent standardized indices of precipitation, evapotranspiration,
680 runoff, surface runoff, baseflow (subsurface runoff) and streamflow, respectively.

681 **Figure 8.** Fractions of uncertainties from internal variability (orange), RCP scenarios
682 (green) and climate and land surface hydrological models (blue) for the projections of
683 20-years moving averaged (a) temperature, (b) precipitation (c) streamflow and (d)
684 hydrological drought frequency. ~~Two dashed lines indicate the multi-model ensemble
685 median years reaching 1.5 °C (year 2025), 2 °C (year 2042) and 3 °C (year 2070)
686 warming levels, respectively.~~

687

688 **Table Captions**

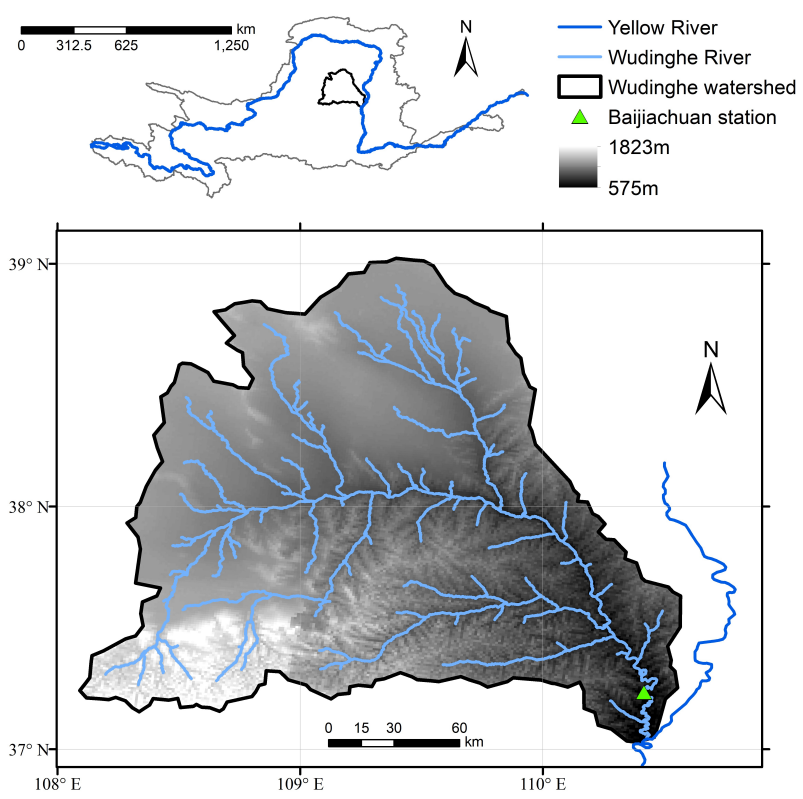
689 **Table 1.** CMIP5 model simulations used in this study. ALL represents historical
690 simulations with both anthropogenic and natural forcings (r1i1p1 realization),
691 RCP2.6/4.5/6.0/8.5 represent four representative concentration pathways from lower
692 to higher emission scenarios.

693 **Table 2.** Trends in hydrometeorological variables and hydrological drought frequency
694 over the Wudinghe watershed. Historical observed trends for streamflow and drought
695 frequency were calculated by using naturalized streamflow data (Yuan et al., 2017).
696 Here, “*” and “**” indicate 90% and 99% confidence levels, respectively, while those

697 without any “*” show no significant changes ($p>0.1$).

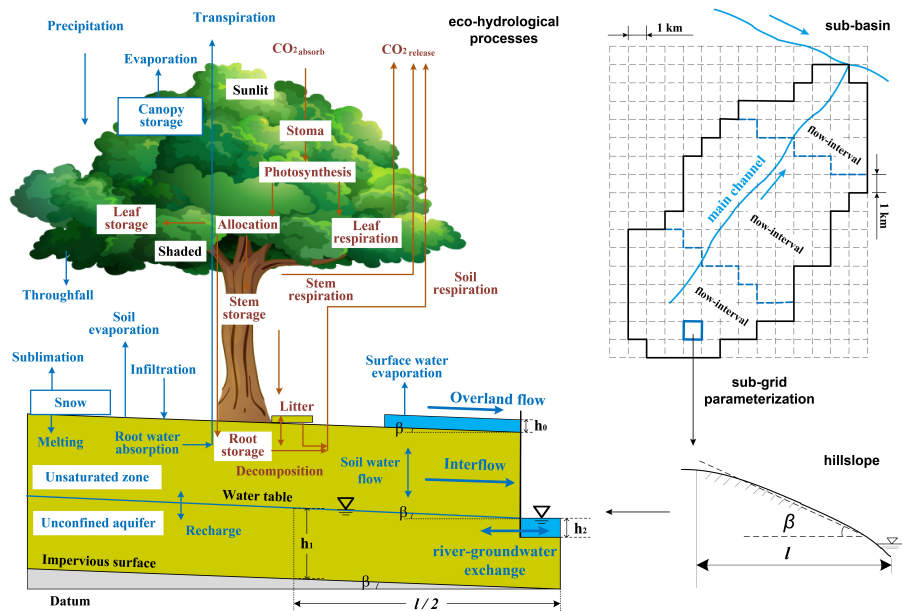
698 **Table 3.** Determination of crossing year for the periods reaching 1.5, 2 and 3 °C
699 warming levels for different GCMs and RCPs combinations. Here, “NR” means that
700 the corresponding GCM/RCP combination will not reach the specified warming level
701 throughout the 21st century.

702 ~~Table 4. Uncertainty contributions (%) from internal variability, climate models and~~
703 ~~RCPs scenarios for the future projections considering 1.5, 2 and 3 °C warming levels.~~



704

705 **Figure 1.** Location, elevation and river networks for the Wudinghe watershed.

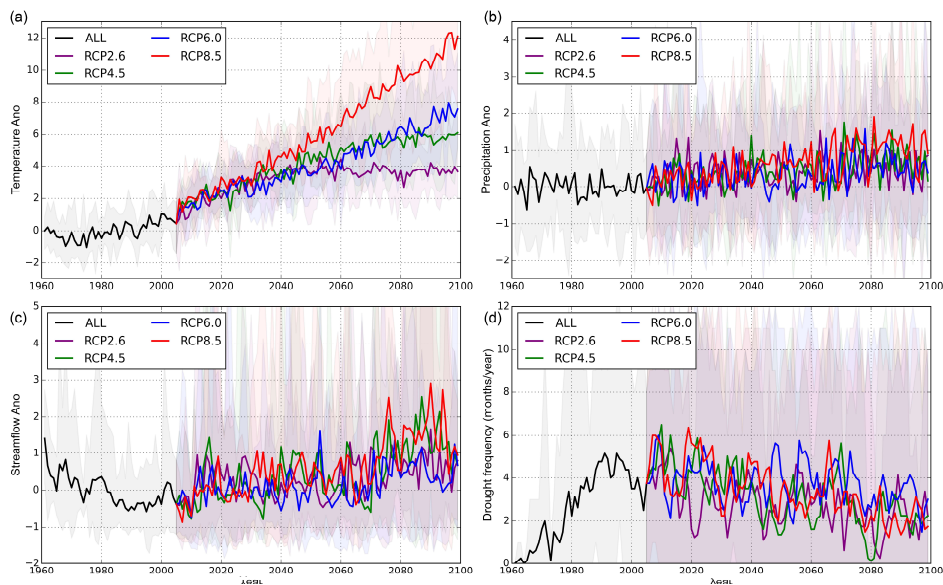


706

707 **Figure 2.** Structure and main eco-hydrological processes for the land surface

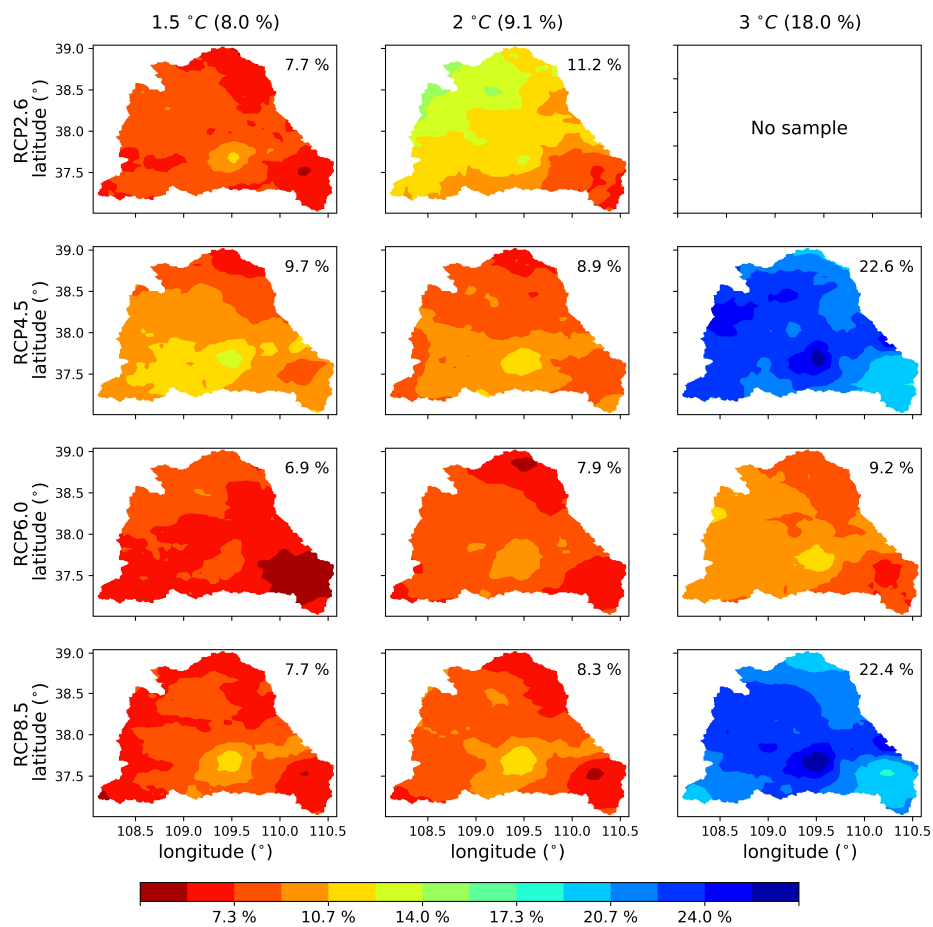
708 hydrological model CLM-GBHM. (modified from Jiao et al., 2017)

709



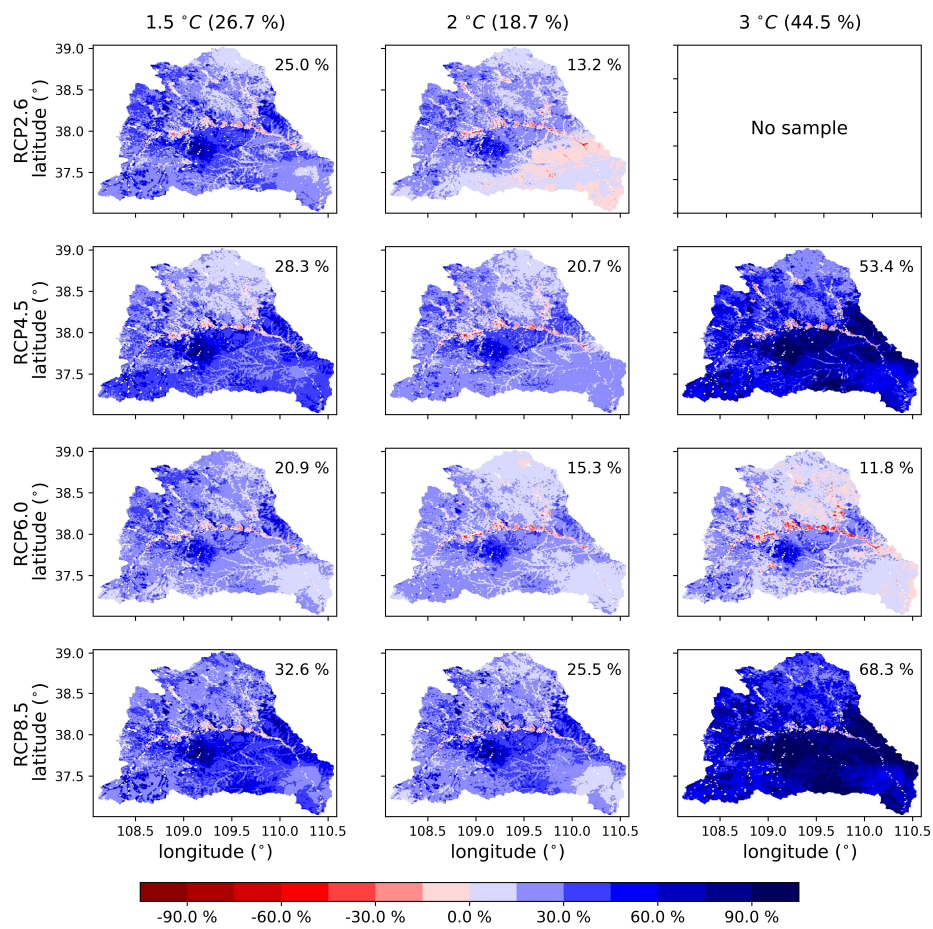
710

711 **Figure 3.** Historical (ALL) and future (RCP2.6/4.5/6.0/8.5) time series of
 712 standardized annual mean (a) temperature, (b) precipitation and (c) streamflow, and (d)
 713 the time series of hydrological drought frequency (drought months for each year) over
 714 the Wudinghe watershed. Shaded areas indicate the ranges between maximum and
 715 minimum values among CMIP5/CLM-GBHM model simulations. ALL represents
 716 historical simulations with both anthropogenic and natural forcings,
 717 RCP2.6/4.5/6.0/8.5 represent four representative concentration pathways from lower
 718 to higher emission scenarios.



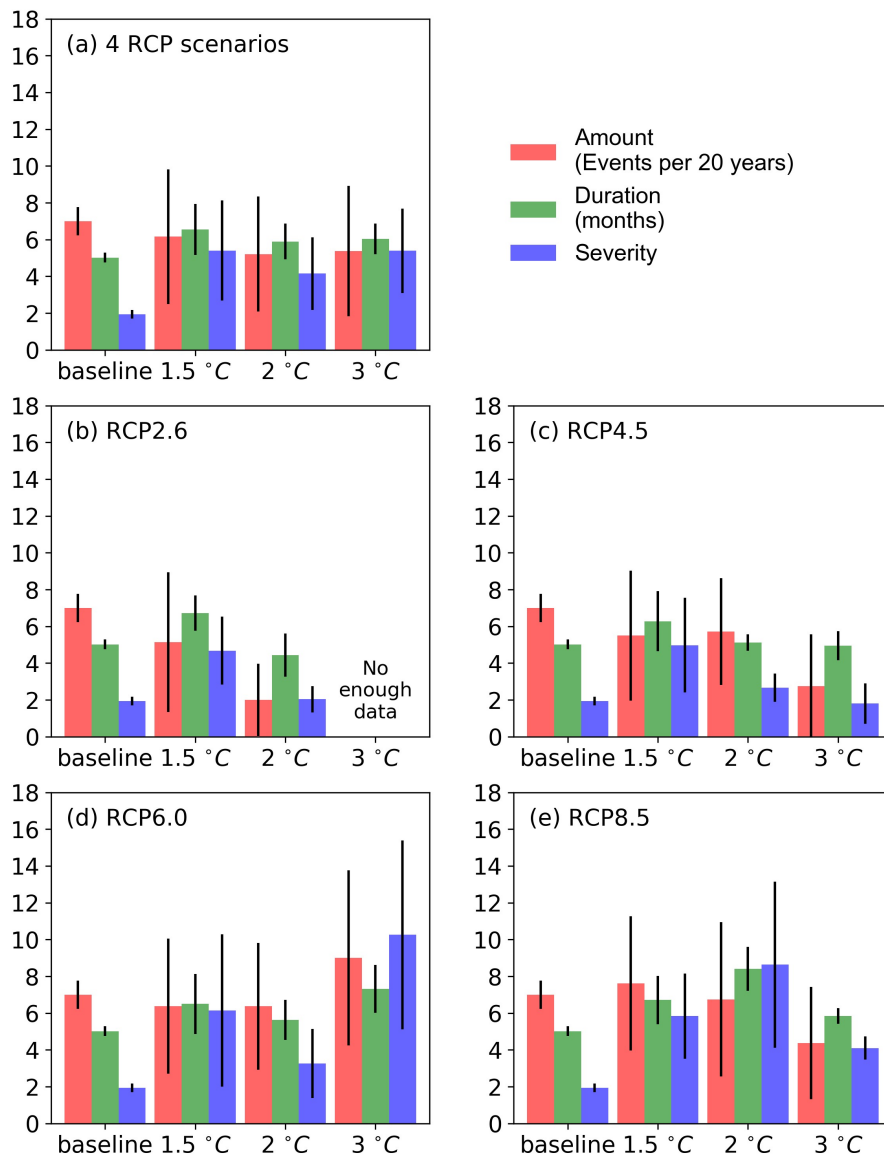
719

720 **Figure 4.** Spatial pattern of relative changes in multi-model ensemble mean
 721 precipitation at 1.5, 2 and 3 °C warming levels compared to the baseline period
 722 (1986-2005). The percentages in the upper-right corners of each panel are the
 723 watershed-mean changes for different RCP scenarios, and the percentages in the top
 724 brackets are the mean values from four RCP scenarios.



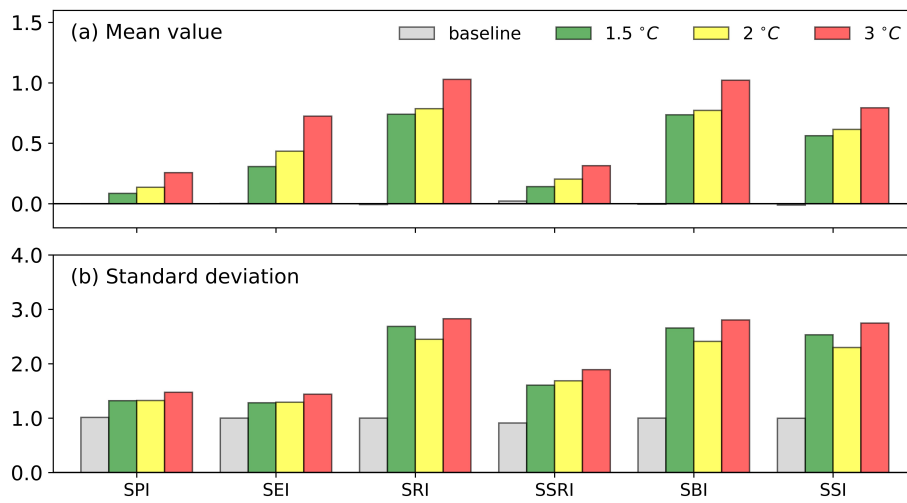
725

726 **Figure 5.** The same as **Figure 4**, but for the spatial patterns of
 727 runoff changes.



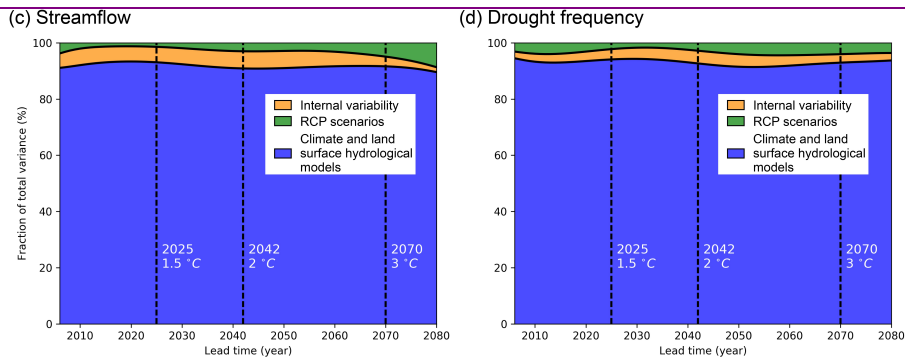
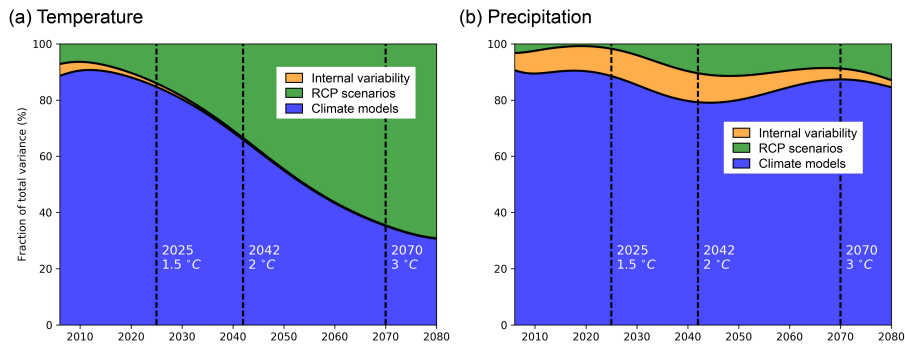
728

729 **Figure 6.** Comparison of the characteristics (amount (number of drought events per
 730 20 years), duration (months) and severity) averaged among climate models and RCP
 731 scenarios for hydrological drought events during the baseline period (1986-2005) and
 732 the periods reaching 1.5, 2 and 3 °C warming levels. Black lines indicate 5%-95%
 733 confidence intervals.

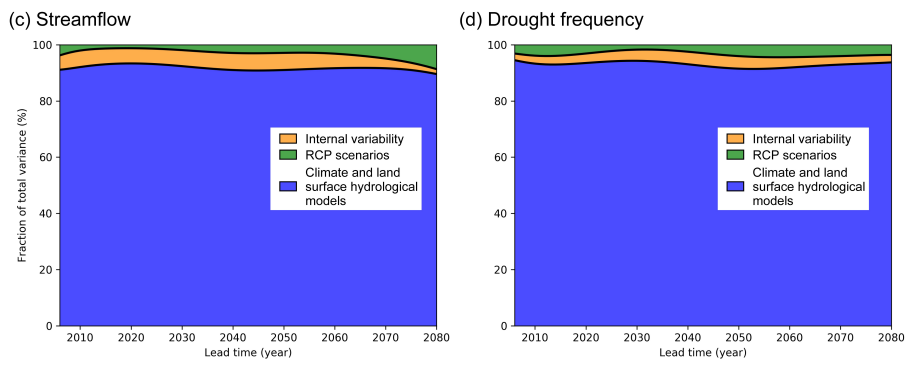
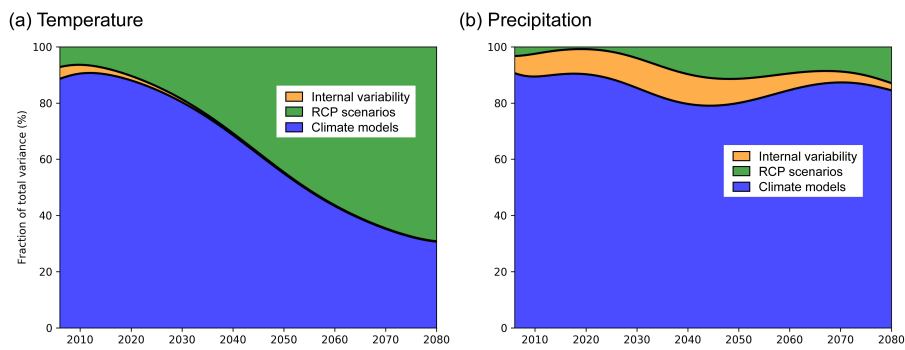


734

735 **Figure 7.** Comparison of (a) mean values and (b) standard deviations for hydrological
 736 indices averaged among climate models and RCP scenarios during the baseline period
 737 (1986-2005) and the periods reaching 1.5, 2 and 3 °C warming levels. SPI, SEI, SRI,
 738 SSRI, SBI, SSI represent standardized indices of precipitation, evapotranspiration,
 739 runoff, surface runoff, baseflow (subsurface runoff) and streamflow, respectively.



740



741

742 **Figure 8.** Fractions of uncertainties from internal variability (orange), RCP scenarios

743 (green) and climate and land surface hydrological models (blue) for the projections of
744 20-years moving averaged (a) temperature, (b) precipitation (c) streamflow and (d)
745 hydrological drought frequency. ~~Two dashed lines indicate the multi model ensemble~~
746 ~~median years reaching 1.5 °C (year 2025), 2 °C (year 2042) and 3 °C (year 2070)~~
747 ~~warming levels, respectively.~~

748 **Table 1.** CMIP5 model simulations used in this study. ALL represents historical simulations with both anthropogenic and natural forcings
 749 (r1i1p1 realization), RCP2.6/4.5/6.0/8.5 represent four representative concentration pathways from lower to higher emission scenarios.

GCMs	Institute	Resolution	Historical simulations	RCP scenarios
GFDL-CM3	NOAA GFDL	144×90	ALL	RCP2.6/4.5/6.0/8.5
GFDL-ESM2M	NOAA GFDL	144×90	ALL	RCP2.6/4.5/6.0/8.5
HadGEM2-ES	MOHC	192×145	ALL	RCP2.6/4.5/6.0/8.5
IPSL-CM5A-LR	IPSL	96×96	ALL	RCP2.6/4.5/6.0/8.5
IPSL-CM5A-MR	IPSL	144×143	ALL	RCP2.6/4.5/6.0/8.5
MIROC-ESM-CHEM	MIROC	128×64	ALL	RCP2.6/4.5/6.0/8.5
MIROC-ESM	MIROC	128×64	ALL	RCP2.6/4.5/6.0/8.5
MRI-CGCM3	MRI	320×160	ALL	RCP2.6/4.5/6.0/8.5

750 **Table 2.** Trends in hydrometeorological variables and hydrological drought frequency over the Wudinghe watershed. Historical observed trends
 751 for streamflow and drought frequency were calculated by using naturalized streamflow data (Yuan et al., 2017). Here, “*” and “**” indicate 90%
 752 and 99% confidence levels, respectively, while those without any “*” show no significant changes ($p>0.1$).

Historical (1961-2005) and future (2006-2099) scenarios	Changing trend of standardized timeseries (yr^{-1})			
	Temperature	Precipitation	Streamflow	Drought frequency
(historical) observations	0.0494**	-0.0216*	-0.0503**	0.0448**
(historical) all forcings simulations	0.0272**	-0.0009	-0.0213**	0.0346**
(future) RCP2.6 simulations	0.0138**	0.0025*	0.0046**	-0.0069**
(future) RCP4.5 simulations	0.0291**	0.0056**	0.0105**	-0.0096**
(future) RCP6.0 simulations	0.0312**	0.0039**	0.0038**	-0.0044**
(future) RCP8.5 simulations	0.0345**	0.0108**	0.0133**	-0.0107**

753 **Table 3.** Determination of crossing year for the periods reaching 1.5, 2 and 3 °C warming levels for different GCMs and RCPs combinations.

754 Here, “NR” means that the corresponding GCM/RCP combination will not reach the specified warming level throughout the 21st century.

GCMs	1.5 °C warming level				2 °C warming level				3 °C warming level			
	RCP2.6	RCP4.5	RCP6.0	RCP8.5	RCP2.6	RCP4.5	RCP6.0	RCP8.5	RCP2.6	RCP4.5	RCP6.0	RCP8.5
GFDL-CM3	2016	2018	2019	2018	2039	2032	2039	2030	NR	2066	2070	2052
GFDL-ESM2M	NR	2051	2059	2038	NR	NR	2076	2054	NR	NR	NR	2084
HadGEM2-ES	2020	2023	2023	2018	2042	2039	2042	2032	NR	2071	2070	2052
IPSL-CM5A-LR	2030	2029	2031	2025	NR	2045	2049	2037	NR	NR	2086	2057
IPSL-CM5A-MR	2032	2025	2031	2024	NR	2045	2050	2037	NR	NR	2081	2055
MIROC-ESM-CHEM	2019	2024	2026	2020	2037	2038	2042	2032	NR	2075	2070	2051
MIROC-ESM	2026	2025	2032	2024	2048	2039	2046	2033	NR	2080	2076	2056
MRI-CGCM3	2075	2043	2053	2036	NR	2074	2070	2049	NR	NR	NR	2072
Model ensemble	2026	2025	2031	2024	2041	2039	2048	2035	NR	2073	2073	2056
Total ensemble	2025 (2016~2075)				2042 (2030~2076)				2070 (2051~2086)			

755

756

Table 4. Uncertainty contributions (%) from internal variability, climate models and RCPs scenarios for the future projections considering 1.5, 2

757

and 3 °C warming levels.

Variables	1.5 °C warming level			2 °C warming level			3 °C warming level		
	Internal- variability	Climate- Models	RCPs- scenarios	Internal- variability	Climate- Models	RCPs- scenarios	Internal- variability	Climate- Models	RCPs- scenarios
Temperature	1.4	84.4	14.3	0.7	66.3	33.0	0.2	36.1	63.7
Precipitation	9.7	87.8	2.5	10.1	80.4	9.5	4.1	86.3	9.6
Streamflow	5.6	92.8	1.6	6.0	91.2	2.8	3.5	91.3	5.1
Drought frequency	3.6	93.8	2.5	4.4	92.8	2.8	3.1	92.8	4.0

758

带格式的：段落间距段后：0 磅

带格式的：两端对齐，行距：2 倍行距，无孤行控制

带格式的：两端对齐，行距：2 倍行距，无孤行控制

带格式的：两端对齐，行距：2 倍行距，无孤行控制，字体对齐方式：自动对齐

带格式的：两端对齐，行距：2 倍行距，无孤行控制

带格式的：两端对齐，行距：2 倍行距，无孤行控制，字体对齐方式：自动对齐

带格式的：两端对齐，行距：2 倍行距，无孤行控制

带格式的：两端对齐，行距：2 倍行距，无孤行控制，字体对齐方式：自动对齐

带格式的：两端对齐，行距：2 倍行距，无孤行控制

带格式的：两端对齐，行距：2 倍行距，无孤行控制，字体对齐方式：自动对齐

带格式的：段落间距段后：0 磅